Simulating three-dimensional dynamics of flexible fibers in a ring spinning triangle: chitosan and cotton fibers

Hui Fen Guo[a], Ngan Yi Kitty Lam[b], Chenxiao Yang[c], and Li Li[d]*

[a] *Institute of Textiles and Clothing*, *The Hong Kong Polytechnic University, Hong Kong*

[b] *Institute of Textiles and Clothing, The Hong Kong Polytechnic University, Hong Kong*

[c] *Institute of Textiles and Clothing*, *The Hong Kong Polytechnic University, Hong Kong*

[d] *Institute of Textiles and Clothing*, *The Hong Kong Polytechnic University, Hong Kong*

*Corresponding author:
Li Li, Institute of Textiles and Clothing, The Hong Kong Polytechnic University, Hung Hom, Kowloon, Hong Kong.
Email: li.lilly@polyu.edu.hk

Simulating three-dimensional dynamics of flexible fibers in a ring spinning triangle: chitosan and cotton fibers

Abstract

A three-dimensional particle-level simulation method is developed to simulate fiber dynamics in the ring spinning triangle. The fiber is modeled as a chain of beads connected through massless rods, and its flexibility is defined by the stretching, bending and twisting displacements. As the application of the proposed approach, the effects of the chitosan (CS)/cotton (CT) fiber initial position and length on fiber motion and yarn properties are discussed. The deflections of CS fibers along the roller axis are larger compared with those of CT fibers, which will lead to CS migrating outwards in CS/CT blended yarn. The short CS fibers (22 mm) will move toward the top roller surface and shift quickly out of the roller nip, and thus yarn strength is lower. The tailing end of the longest CS fiber (46 mm) will drift off the roller nip, which makes little or no contribution to the yarn strength. For 38 mm length CS fiber, it moves toward the bottom roller surface and is bound into the roller nip, and thus can produce the highest tenacity CS/CT blended yarns. The simulation results agree with the spinning experimental data reported by other researchers.

Keywords

chitosan fiber, fiber configuration, roller, spinning triangle, yarn

In the ring spinning process, the drafted strand leaves the front roller nip and is twisted into a yarn. This twist region between the front roller nip and the fiber convergence point is called the spinning triangle. This triangle zone influences the distribution of fiber tensions and the properties of spun yarns, especially the yarn strength, torque and hairiness.[1,2]Consequently, increased attention is being paid to the subject of the spinning triangle in order to produce a high quality yarn. At present, most of the information available in the literature on the spinning triangle is based on spinning experiments and theoretical models.[1–5] Obviously, the formation of the triangle zone, that is, the fiber distribution, is closely related to the fiber dynamics in the airflow created by the rotating front roller-pairs and the air suction system. In this triangle, due to the interaction of the airflow–fiber and fiber–fiber, the flexible fibers

are transferred and rotated around the neighboring fibers, resulting in the fibers twisting into the convergence point. This is an air/fiber two-phase problem. To the authors' knowledge, however, studies in this area are rather scarce. Therefore, in this paper, we will study the fiber dynamics in the airflow of a spinning triangle using a numerical method based on multiphase flow, and discuss the formation principle of the triangle zone.

Due to the inherent complexity of the textile industry, little work has been reported regarding the air–fiber flow in the textile area. Considering a fiber as a series of contiguous two-dimensional (2D) elastica, Smith and Roberts[6] computed the fiber motion in converging transport ducts. Kong and Platfoot[7] developed a 2D Lagrangian one-way coupling model to simulate fiber transportation in the transfer-channel of rotor spinning and evaluated the effect of circulation zones and the number of nodes of the fiber on fiber configurations. In their model, a fiber consisted of a discrete distribution of masses held together by weightless chains. Nevertheless, this model would not give a clear picture of elastic deformation of the fiber. To study the fiber motion in high-speed airflow of the air-jet spinning nozzle, Zeng and Yu[8] proposed a 2D bead-rod fiber model that was made up of beads connected by massless rods, by changing the distance and the bending deflection in successive rods to mimic bending and twisting. Pei and Yu[9] adopted a 2D arbitrary Lagrangian–Eulerian fluid–structure interaction model combined with the fiber–wall contact to simulate the fiber motion inside the nozzle of Murata vortex spinning. However, their prediction[6–9] cannot show some properties of fiber dynamics, since the airflow fields and flexible fiber deformations are three dimensional (3D). In order to investigate more deeply the fiber dynamics, it is necessary to study 3D air–fiber flow in the textile industry.

The textile fibers differ from the general particulates by such properties as large aspect ratio, elasticity and flexibility. To reduce computational demands, particle-level simulation, where fibers are represented by a multi-rigid-body chain, such as a bead chain,[10] a needle chain[11,12] or a bead-rod chain,[13] is an alternative tool. The advantage of such models is that they look at phenomena occurring at the scales of the length of a single fiber. Flexibility of the fibers in these models can be obtained and changed according to the parameters of bond stretching, bending and twisting. Therefore, a 3D particle-level simulation can study well air–fiber dynamics in the textile area. For example, based on particle-level simulation, Guo and Xu[13] introduced a 3D bead-rod chains fiber model to calculate the flexible fiber motions in air-jet

spinning with two nozzles[14,15]and discussed the principle of the air-jet yarn formation.[13] In their model, only bending and twisting of the fiber were molded. However, fiber extensibility, which affects fiber tension, is important in the spinning triangle. Therefore, in this study, we will extend the 3D fiber model of Guo et al.[13–15] to consider fiber extensibility. This proposed method is applied to the prediction of 3D motions of chitosan (CS) and cotton (CT) fibers in a ring spinning triangle, and we discuss the effects of the length and position of CS fibers on the CS/CT blended yarn properties. Consequently, the spinning experiments of Lam et al.[16] and the formation principle of the triangle zone are demonstrated.

Theory

To simulate a fiber motion in an airflow field in the spinning triangle, the one-way coupling Euler–Lagrange approach is utilized. The flow field is firstly obtained by solving Navier–Stokes equations using the finite-volume approach,[17] and then fiber dynamics is investigated by solving the bead-rod model equations describing the response of an elastic fiber to the combined forces exerted on it by the fluid flow.

In the ring triangle zone, the airflow will be created by the opposite direction rotating front roller-pairs and the air suction system whose outlet is close to the nip of the rollers. If we consider a 3D suction flute, it will greatly increase the difficulties of the geometrical modeling and (the converging) simulation due to the negative pressure. In this paper, only the flow field cause by rotating the roller-pair, which is simplified as circular cylindrical shapes, is simulated. Figure 1 shows the profile with two rotating cylinders used in a 3D simulation. The origin of the 3D Cartesian coordinate system is located at the center of the axis of the upper cylinder (the top roller) without the offset. The *z*-axis is along the axial direction of the upper cylinder and the *y*-axis is vertical pointing downwards. For the airflow field, the numerical formulation of the problem and the flow characteristics have been fully described by Guo et al.[17]

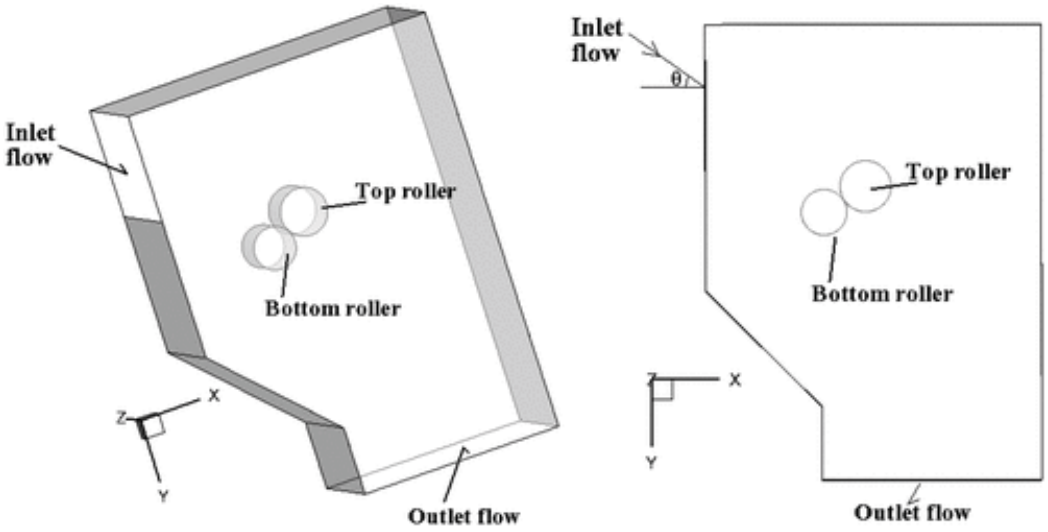

Figure 1. Profiles of the three-dimensional model and *z*-direction projection.

The dynamics of a flexible fiber in a flow field depends on the fiber properties, such as stiffness, fiber length, the surface roughness and cross-sectional deformation. To simplify this, the surface roughness and cross-sectional deformation of the fiber are ignored and a fiber with equal diameter and smooth surface is assumed. Here the fiber is composed of *n*beads of radius *r* that are connected by $n-1$ massless rods.[13–15] In the proposed model, only the beads are affected by forces, and the rods serve to transmit forces and maintain the configuration of the fiber. Therefore, the calculation of the fiber dynamics by the Lagrangian approach requires the solution of the equation of motion for each bead. According to Newton's second law, the equations of motion for the bead *i* render

$$m_i d\mathbf{V}_i/\mathrm{dt} = \mathbf{F_i^i} + \mathbf{F_i^e} \qquad d\mathbf{x}_i/\mathrm{dt} = \mathbf{V}_i \tag{1}$$

where m_i, $\boldsymbol{V}_i$ and $\boldsymbol{X}_i$ represent the mass, velocity and displacement of bead *i*, respectively. The resultant internal force F_i^i is the combination of the stretching F_i^s, bending F_i^b and twisting F_i^t restoring forces. Ignoring other hydrodynamic forces, such as the Basset history term, added mass, slip-rotational lift force and fluid inertia, the resultant external force F_i^e only consider drag force.

Based on small deflection theory,[18] Guo et al.[13–15] simulated the fiber bend and twist, which can be described by changing the displacements of three or four adjacent beads,

respectively (Figures 2(b) and (c)). Similarly, as the extension the 3D fiber model of Guo et al.,[13–15] the fiber stretch is considered by changing the displacement of two adjacent beads here (Figure 2(a)). The stretching F_i^s, bending F_i^b and twisting F_i^t restoring forces exert on the bead i as follows

$$\mathbf{F}_i^s = \frac{\pi r^2 E}{l_{i-1,i}} \Delta l \mathbf{e}_{i-1,i}$$

$$\mathbf{F}_i^b = -\frac{3\mathrm{EI}_b}{l_{i-1,i}^3} \mathbf{s}_b \tag{2}$$

$$\mathbf{F}_\mathrm{i}^\mathrm{t} = -\frac{\mathrm{GI}_t}{l_s l_{i-2,i-1}} \mathbf{s}_t$$

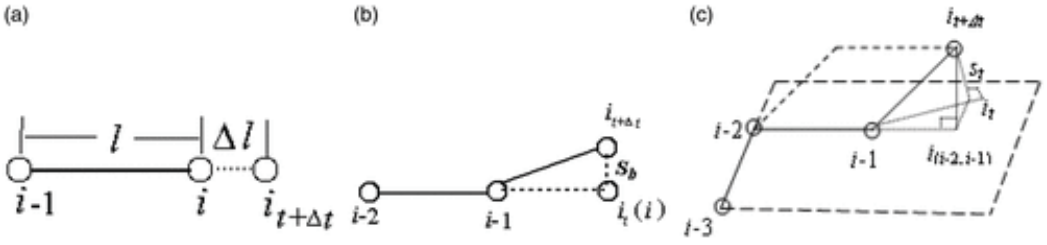

Figure 2. Sketch of the fiber deformations for (a) stretching, (b) bending and (c) twisting. Note that (b) and (c) are used in Guo et al.'s model.[13–15]

As shown in Figure 2, Δl and $\boldsymbol{e}_{i-1,i}$ are the extension and unit vectors of the fiber section $(i-1, i)$, respectively. $(i-1, i_t)$ is the equilibrium position of the fiber section $(i-1, i)$, and the fiber section will be bent when bead i moves from i_t to $i_{t+\Delta t}$. The fiber section $(i-1, i_{t+\Delta t})$ is the position after torsion of $(i-1, i)$ and the line $(i_{t+\Delta t}, i_t)$ is normal to the plane comprising of fiber sections $(i-2, i-1)$ and $(i-3, i-2)$. $\boldsymbol{s_b}$ is the bending deflection of the section $(i-1, i)$ and $\boldsymbol{s_t}$ is the twisting displacement of the section $(i-2, i-1)$. E and I_b are the Young's modulus and the moment of inertia of the fiber cross-section area, respectively. G and I_t are the shear modulus and the polar moment of inertia, respectively. $l_{i-1,i}$ and $l_{i-2,i-1}$ are the fiber lengths from its adjacent beads $i-1(i-2)$ and i $(i-1)$, respectively. l_s is the length of the line segment $(i_{t+\Delta}, i_{(i-2,i-1)})$.

For bead i, these forces are contributed by fiber sections $(i-1, i)$ and $(i, i+1)$, and can be calculated by the following

$$\mathbf{F}_i^d = (\mathbf{F}_{i-1,i}^d + \mathbf{F}_{i,i+1}^d)/2 \tag{3}$$

$F_{i-1,i}^d$ and $F_{i+1,i}^d$ are the drag forces acting on bead i, which are devoted to fiber sections $(i-1, i)$ and $(i, i+1)$,respectively. To obtain these forces, the method of equivalent volume is used to calculate the drag force exerted on the cylindrical particle. The drag $F_{i-1,i}^d$acting on the fiber section $(i-1, i)$ can be expressed as follows

$$\mathbf{F}_{i-1,i}^d = \pi d_v^2 C_D \rho_g \left|\mathbf{V}_{\mathrm{gi}} - \mathbf{V}_{\mathrm{fi}}\right| (\mathbf{V}_{\mathrm{gi}} - \mathbf{V}_{\mathrm{fi}})/8 \tag{4}$$

where $\boldsymbol{V}_{gi}$ and $\boldsymbol{V}_{fi}$ are the fluid and fiber velocities at the mass center of the fiber section $(i-1, i)$, respectively. $d_v = (6r^2 l_{i-1,i})^{1/3}$ is the equivalent diameter of an equal volume sphere. C_D is the drag coefficient.

Since the gap between two cylinders (roller nip) is very small, the fiber will frequently touch two cylinder walls; thus, a simple particle-wall collision model by Grant and Tabakoff[19] is adopted

$$e_{\mathrm{n}} = 0.993 - 1.76\alpha + 1.56\alpha^2 - 0.49\alpha^3$$

$$\mathrm{e_t} = 0.988 - 1.66\alpha + 2.11\alpha^2 - 0.67\alpha^3 \tag{5}$$

where e_n and e_t are normal and tangential coefficients of restitution on the collision angle, α, respectively.

To eliminate the probability of the beads overlapping, the time step Δt is chosen so that the beads traverse no more than 20% of the fiber diameter in each step. The computation will end when the following condition is satisfied[20]

$$\sum_{i=0}^{\mathrm{n}} \left|\mathbf{X}_i^{n+1} - \mathbf{X}_i^n\right| < 10^{-6} \tag{6}$$

where X_i^n and X_i^{n+1} are the displacements of bead i at times t^n and t^{n+1} , respectively.

Results and discussion

Due to their biodegradability, biocompatibility, antimicrobial activity and non-toxicity, CS fiber can be used to make functional materials and fabrics in the textile area.[21] However, the use of CS has been limited due to its poor mechanical properties, moisture sensitivity and poor spinnability. The blending of CS/CT fiber in a ring spinning system is an alternative way for improving the pure CS yarn strength. The spinning experiments by Lam et al.[16] supported this well. In their experiments, the effect of the CS length on the blended CT/CS yarn was also discussed. In this section, we will use the proposed approach to simulate the fiber motions in a spinning triangle, and analyze the effects of the position and length on yarn properties. Therefore, the formation principle of the triangle zone and the experiments of Lam et al.[16] can be demonstrated from the multiphase flow view.

For all the following studied cases, the fiber is placed initially in an inclined plane between two cylinders (the roller nip), which has an angle from the horizontal plane due to the inclination of the drafting system (Figure 3). The trailing end of the fiber is outside the front roller nip and its leading end is still inside it. Along the z-axis (the roller length), the fibers at the two different initial positions, that is, at/near the center of the roller (z = 0 and 5 mm), are computed. It is noted that the cylinder length is 28 mm and only the fibers at one side of the cylinder center are simulated. Based on the experiments of Lam et al.,[16] the CT length is L_{CT} = 38 mm and the CS lengths are L_{CS} = 22, 30, 38, 46 mm, respectively . The initial velocity of the bead that constitutes the fiber is equal to that of the fluid at the location of the bead centroid. The computations will be completed with MATLAB programming.

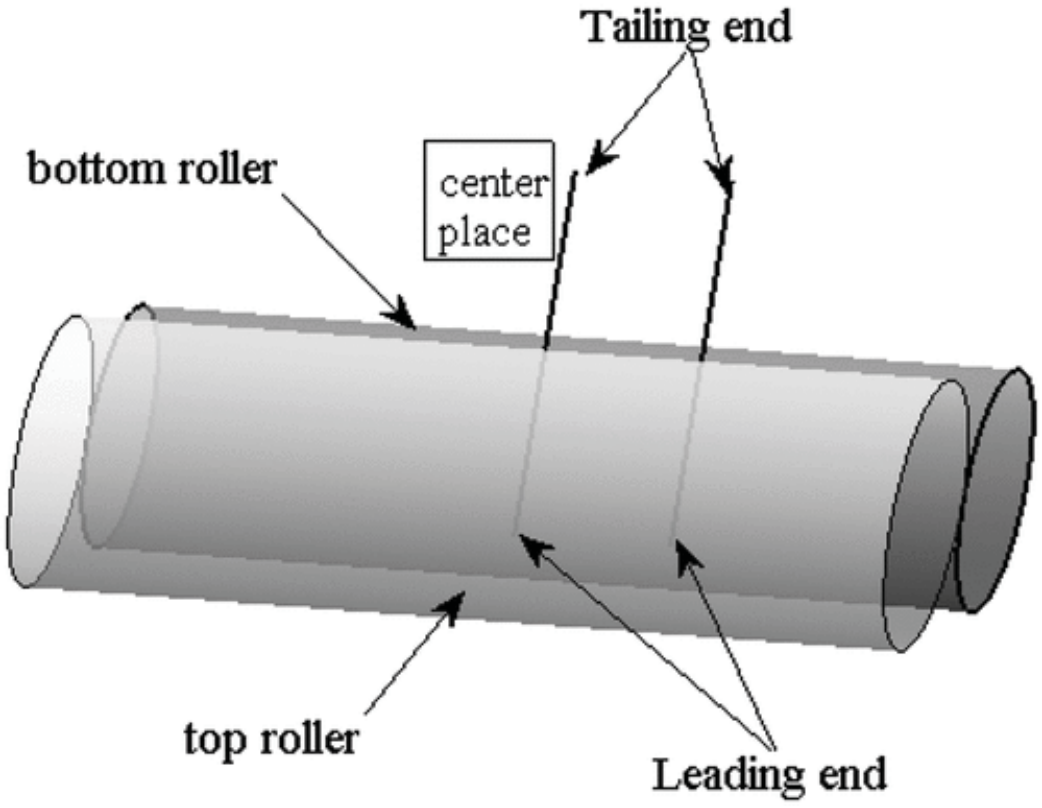

Figure 3. The initial positions of the computed fibers.

As shown in Figure 4, owing to the two cylinders rotating in the opposite direction, the velocity is the largest near the circular cylinders, the stream-wise directions of the fluid around two cylinders are opposite and the counter-rotating vortex pair in the upper part of the roller is asymmetric.[17] Therefore, the tailing end of the center CS fiber ($z = 0$ mm) with 38 mm length deflects gradually from the cylinder center. However, the fiber is bound into the roller nip and its head-end moves toward both the z-axis center and the bottom roller to form the spinning triangle.[22] It is also noted that the fiber moves along the stream-wise direction and rotates in a spiral orbit. This is because the rotating flow is a helical flow. The fiber shifts like a leaf-spring until its leading end begins to bend; after that the deformation of the fiber is slightly flexible and forms a snake configuration;[23] finally, the fiber will straighten gradually in the triangle zone (see Figure 4(b)). This coincides with the formation principle of the triangle zone[22] that the fiber assembly contains no twist in this zone.

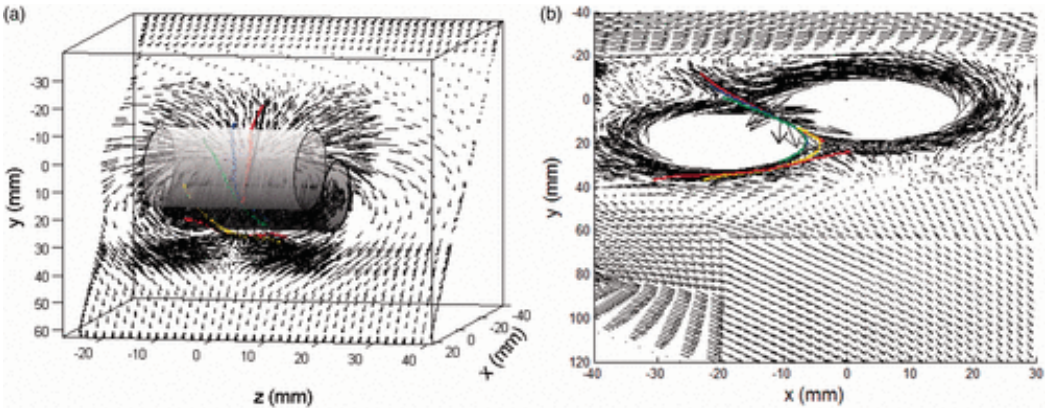

Figure 4. Fluid velocity vector and evolutions of the 38 mm center ($z = 0$ mm) chitosan fiber configurations: (a) three-dimensional and (b) *xy*-plane projection. The colored thick lines indicate the fiber shapes at different times. The short black lines with arrows indicate the fluid velocity vectors. (Color online only.)

Figure 5 shows the trajectories of end beads of 38 mm CS and CT fibers with different initial positions. For all fibers, along the *z*-axis, their tailing ends first move in the opposite direction of the axis, then toward the cylinder center, which forms a helical trajectory. Similarly, the leading end bead also moves as a helix. Again, except the leading end of the CT fiber at $z = 5$ mm, they are bound into the cylinder nip and cover onto the surface of the bottom cylinder. Consequently, the triangle zone is formed, in which the fibers move toward the axis centre (convergence point). It is clear that for the CT fibers, the *z*-direction deflections of their tailing end are very much smaller than those of CS fibers due to the smaller flexible rigidity of CT fibers; thus, the pure CT yarn can form a narrower and longer triangle compare to the pure CS yarn. According to the principle of ring spinning,[22] the small triangle width can make the edge fibers are better bound in the yarn, which gives smoother (less hairy) and stronger yarns. Hence, the pure CT yarn will show higher yarn tenacity than that of the pure CS yarn. Likewise, the simulation results also show that CS fibers will migrate outwards in CS/CT blended yarn due to the larger z-direction offset of the CS fibers. This coincides with the observation indicated by Lam et al.,[16] who observed that Hamilton migration indexes[24] of CS fibers are positive (i.e. outward migration) for all CS/CT blended yarn.

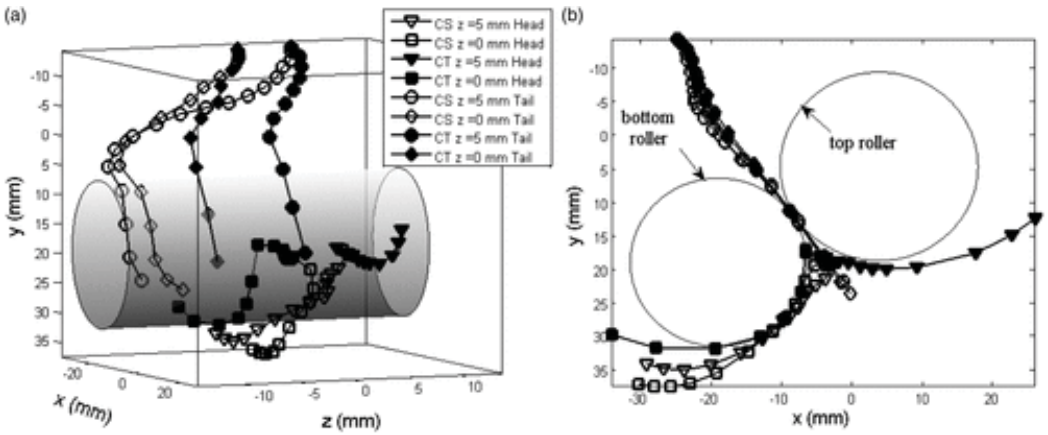

Figure 5. The trajectories of two end beads of 38 mm chitosan (CS) and cotton (CT) fibers with different initial positions: (a) three dimensional; (b) projection on the *xy*-plane.

The fiber length plays an important role in judging yarn properties. Figure 6 shows the trajectories of CS fibers near the roller center ($z = 5$ mm) with the length $L_{CS} = 22$ and 46 mm. All fibers with springy and snake-like configurations move along the stream-wise direction. Too short fiber ($L_{CS} = 22$ mm) will shift quickly out of the roller nip and move toward the top roller with a snake shape, thus forming fly.[22] This is because a short fiber generates a smaller frictional resistance to an external force. Different from short fibers, of which length is less than or equal to 38 mm (see also Figures 4 and 5), longer fiber ($L_{CS} = 46$ mm) at $z = 5$ mm drifts toward the same direction of its initial position along the roller (z-)axis and moves toward the top roller surface. It is also noted that the movement distance of the long fiber is small, which may be because the long fiber has a greater flexible and frictional resistance.[22] This will prolong the residence time of the fibers and cause the entanglement of fibers; consequently, yarn strength will decrease (see also Figure 7). Lam et al.[16] also achieved these results in spinning experiments. They observed that the strength of CS/CT blended yarn with 46 mm CS is the lowest for all yarn samples blended with different length CS fibers.

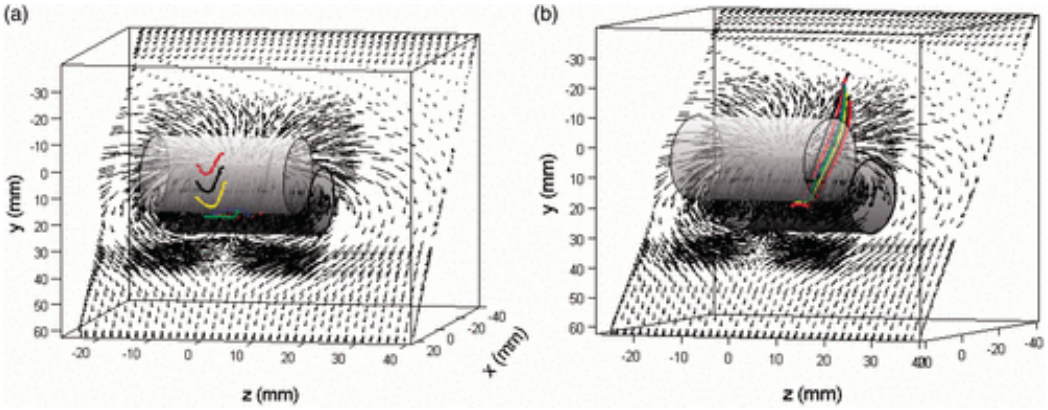

Figure 6. Fluid velocity vector and evolutions of three-dimensional chitosan fiber configurations near the center ($z = 5$ mm) with different fiber lengths: (a), $L_{CS} = 22$ mm; (b) $L_{CS} = 46$ mm. The colored thick lines indicate the fiber shapes at different times and the short black lines with arrows indicate the fluid velocity vectors. (Color online only.)

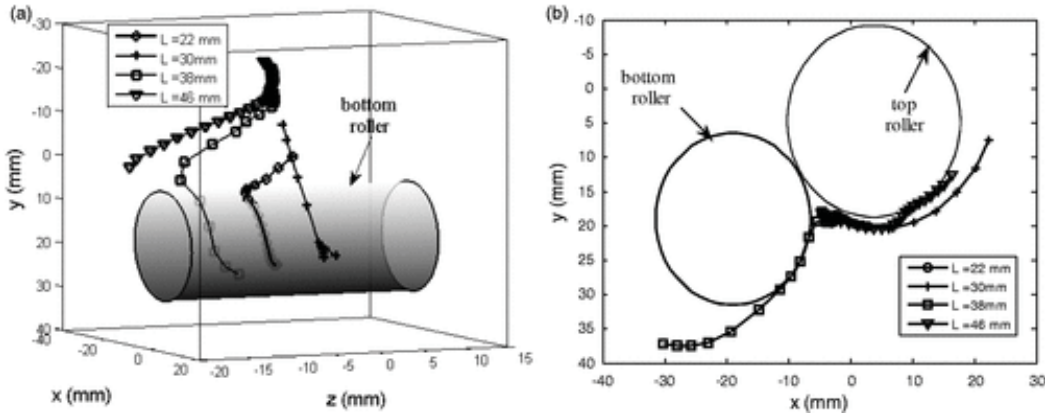

Figure 7. The trajectories of two end beads of chitosan fibers with different lengths at the roller center: (a) three-dimensional tailing end beads; (b) projection on the *xy*-plane of leading end beads.

To further study the effect of the fiber length, Figure 7 shows the trajectories of two end beads of CS fibers with different lengths at the roller center. Except the fiber with the length $L_{CS} = 38$ mm, the leading end beads of the CS fibers move around the top roller surface, which will form leading end hair. Similar to the 38 mm length CS fiber, the tailing ends of the CS fibers with the length $L_{CS} = 22$ and 30 mm also deflects gradually from the cylinder center due to the *z*-direction asymmetric fluid of the rotating flow (see also Figures 4 and 6) and the fibers are bound into the roller nip. It is also noted that the CS fiber with 30 mm length deflects a smaller distance along the *z*-axis compared with that of other fibers, and its leading end has an entanglement

in the roller nip. Consequently, yarn tenacity increases slightly. The simulation results show that the CS/CT blended yarns spun using 38 mm length CS fibers show the highest tenacity (see also Figures 5 and 6), which agrees well with the spinning experimental results presented by Lam et al.[16] For the longest CS fiber ($L_{CS} = 46$ mm), its tailing end bead drifts off the roller nip, that is, out of the cylinders, and its leading portion moves around the top roller (upper cylinder). Therefore, two end portions of the fiber ($L_{CS} = 46$ mm) will form hair and make little or no contribution to the yarn strength. These results coincide with the observation indicated by Salhotra et al.,[25] who experimentally observed that the yarn tenacity increases initially with the increase in fiber length up to 38 mm and then it drops with further increase in fiber length.

Conclusions

The extend bead-rod fiber model proposed by Guo et al.[13–15] was applied to simulate 3D CS/CT fiber dynamics in a ring spinning triangle. The effects of the fiber position and length also discussed. The fiber was modeled as a bead-rod chain, whose motion was determined by solving the translational equations of motion for each bead.

All fibers with springy and snake-like configurations move along the stream-wise direction and rotate as a helical orbit. Again, the fibers also deflect along the *z*-direction (roller axis). The *z*-direction deflections of CS fibers are large compared with those of CT fibers. Therefore, CS fibers will migrate outwards in CS/CT blended yarn, which is supported by the spinning experiments of Lam et al.[16] The shortest fiber ($L_{CS} = 22$ mm) will move around the top roller surface or shift quickly out of the roller nip, resulting in fly fiber. Similarly, the leading end of the longest CS fiber ($L_{CS} = 46$ mm) also covers onto the surface of the top roller, but its tailing end bead will drift off the roller nip or at the same direction, which makes little or no contribution to the yarn strength; thus, yarn strength with 46 mm CS fibers is the lowest in the studied cases. For 38 mm length CS fiber, it moves toward the bottom roller surface and is bound into the roller nip. Consequently, the highest tenacity CS/CT blended yarns will be spun using 38 mm fibers. These results coincide with the observation indicated by other researchers, such as Salhotra et al.[25] and Lam et al.[16]

Declaration of conflicting interests

The authors declared no potential conflicts of interest with respect to the research, authorship and/or publication of this article.

Funding

The authors disclosed receipt of the following financial support for the research, authorship, and/or publication of this article: This work was supported by the Research Grants Council (RGC) of Hong Kong, China (project number: RGC Ref No.PolyU 5420/13H) and by the China Postdoctoral Science Foundation funded project (grant number 2013M540274).

References

1. Tao H, Tao X, Cheng KPS, et al. Effects of geometry of ring spinning triangle on yarn torque Part I: analysis of fibre tension distribution. *Text Res J* 2007; 77: 853–863.
2. Feng J, Xu BG, Tao XM, et al. Theoretical study of spin- ning triangle with its application in a modified ring spin- ning system. *Text Res J* 2010; 80: 1456–1464.
3. Krause HW, Soliman HA and Tian JL. Investigation of the strength of the spinning triangle in ring spinning. *Melliand Textillberichte* 1991; 72: 499–502.
4. Su XZ, Gao WD, Liu XJ, et al. Theoretical study of fiber tension distribution at the spinning triangle. *Text Res J* 2013; 83: 1728–1739.
5. Wang XG and Chang LL. Reducing yarn hairiness with a modified yarn path in worsted ring spinning. *Text Res J* 2003; 73: 327–332.
6. Smith AC and Roberts WW. Straightening of crimped and hooked fibers in converging transport ducts: computa- tional modeling. *Text Res J* 1994; 64: 335–344.
7. Kong LX and Platfoot RA. Computational two-phase air/ fiber flow within transfer channels of rotor spinning machines. *Text Res J* 1997; 67: 269–278.
8. Zeng YC and Yu CW. Numerical simulation of fiber motion in the nozzle of an air-jet spinning machine. *Text Res J* 2004; 74: 117–122.
9. Pei ZG and Yu CW. Numerical study on the effect of nozzle pressure and yarn delivery speed on the fiber motion in the nozzle of Murata vortex spinning. *J Fluids Struct* 2011; 27: 121–133.
10. Yamamoto S and Matsuoka T. A method for dynamic simulation of rigid and flexible fibres in a flow field. *J Chem Phys* 1993; 98: 644–650.
11. Xiang P and Kuznetsov AV. Simulation of shape dynam- ics of a long flexible fiber in a turbulent flow in the hydro- entanglement process. *Int Commun Heat Mass Transfer* 2008; 35: 529–534.
12. Skjetne P, Ross RF and Klingenberg DJ. Simulation of single fiber dynamics. *J Chem Phys 1997*; 107: 2108–2121.
13. Guo HF and Xu BG. A 3D numerical model for a flexible fiber motion in compressible swirling airflow. *CMES Comput Model Eng Sci* 2010; 61: 201–222.
14. Guo HF, Xu BG, Yu CW, et al. Simulating the motion of a flexible fiber in 3D tangentially injected swirling airflow in a straight pipe—effects of some parameters. *Int J Heat Mass Transfer* 2011; 54: 4570–4579.
15. Guo HF, Yu CW, Xu BG, et al. Effect of the geometric parameters on a flexible fiber motion in a tangentially injected divergent swirling tube flow. *Int J Eng Sci* 2011; 49: 1033–1046.

16. Lam NYK, Zhang M, Guo HF, et al. Effect of fibre length and blending method on tensile properties of ring spun chitosan-cotton blend yarns. *Text Res J* 2017; 87(2): 244–257.
17. Guo HF, Lam NY, Yan F, et al. Numerical study of the three-dimensional preliminary flow field in the ring spin- ning triangle. *Text Res J* 2016; 86(16): 1728–1737.
18. Gere JM and Timoshenko SP. *Mechanics of materials,* 2nd ed. London: Van Nostrand, Reinhold, 1987.
19. Grant G and Tabakoff W. Erosion prediction in turbo- machinery resulting from environmental solid particles. *J Aircraft* 1975; 12: 471–478.
20. Autrusson N, Guglielmini L, Lecuyer S, et al. The shape of an elastic filament in a two-dimensional corner flow. *Phys Fluids* 2011; 23: 063602-1-7.
21. Lim SH. Synthesis of a fiber-reactive chitosan derivative and its application to cotton fabric as an antimicrobial finish and a dyeing-improving agent. PhD Dissertation, North Carolina State University, USA. 2002.
22. Lawrence CA. *Advances in yarn spinning technology*. Cambridge, UK: Woodhead Publishing Limited, 2010.
23. Forgacs SGM. Particle motions in sheared suspensions: IX. Spin and deformation of threadlike particles. *J Colloid Sci* 1959; 14: 457–472.
24. Hamilton JB. Radial distribution of fibers in blended yams. Part 1. Characterization by a migration index. *J Text Inst* 1958; 49: T411–T423.
25. Salhotra KR and Alaiban TS. Effect of fibre length on the quality of rotor yarns. *Ind J Fibre Text Res* 1984; 9: 1–3.